



Title	Stroboscopic sampling moiré microscope (SSMM) for investigating full field in-plane vibration of MEMS mechanical transducers
Author(s)	Yadi, Mona; Uenohara, Tsutomu; Mizutani, Yasuhiro et al.
Citation	Precision Engineering. 2025, 92, p. 21-29
Version Type	VoR
URL	https://hdl.handle.net/11094/100207
rights	This article is licensed under a Creative Commons Attribution-NonCommercial-NoDerivatives 4.0 International License.
Note	

The University of Osaka Institutional Knowledge Archive : OUKA

<https://ir.library.osaka-u.ac.jp/>

The University of Osaka



Stroboscopic sampling moiré microscope (SSMM) for investigating full field in-plane vibration of MEMS mechanical transducers

Mona Yadi ^{a,*}, Tsutomu Uenohara ^a, Yasuhiro Mizutani ^a, Yoshiharu Morimoto ^b, Yasuhiro Takaya ^a

^a Department of Mechanical Engineering, Graduate School of Engineering, Osaka University, 2-1 Yamadaoka, Suita, Osaka 565-0871, Japan

^b 4D Sensor Inc., 579-1, Umehara, Wakayama 640-8550, Japan

ARTICLE INFO

Keywords:

MEMS mechanical transducer
Dynamic properties
In-plane vibration measurement
Ultrafast stroboscopic system
Atomic force microscopy (AFM)
Quartz tuning fork (QTF)

ABSTRACT

Precise analysis of the full-field in-plane vibration of microelectromechanical system (MEMS) transducers is crucial for assessing their device functionality and performance. As an example, in the context of frequency/amplitude modulation of Quartz Tuning Fork (QTF)-based atomic force microscopy (AFM) systems, understanding QTF's in-plane vibration can significantly enhance accurate evaluation of tip-sample forces. Current methods, such as analytical and numerical approaches, have limitations when it comes to providing accurate measurements. To address these limitations, we proposed an experimental approach that combines stroboscopic and sampling moiré (SM) techniques. This method focuses on investigating the in-plane vibration of a QTF and utilizes the obtained results to measure the sensor's dynamic properties such as vibration mode shape, resonance frequency (f_0), and quality factor (Q). Nanometer-scale light pulses, generated using a custom-designed stroboscope, are synchronized with the QTF's excitation voltage to freeze the vibration effectively, enabling imaging using a standard CCD camera. Subsequently, SM analysis is employed to extract the surface vibration profile, facilitating the measurement of vibration mode shape, f_0 , and Q . This technique shows promise for analyzing the dynamic behavior of various micro-devices compatible with the sample preparation process.

1. Introduction

Studying microelectromechanical system (MEMS) transducers holds immense significance, as it paves the way for groundbreaking solutions across various domains such as healthcare, communications, transportation, energy, and more. It empowers the creation of smaller, smarter, and more efficient devices, fostering advancements that can elevate our daily lives and drive technological innovation. Vibration analysis is a significant part of this field of research. Vibration theory is intricately linked to model parameters, specifically, frequency, damping, and mode shapes. Conversely, physical systems are characterized by their structural properties, including mass, stiffness, and damping. These model parameters find their roots in the solution of the homogeneous segment of the differential equation of motion for a physical structure, which is expressed in terms of acceleration, velocity, and displacement. Consequently, any alterations in the physical properties of the structure, whether due to damage, external forces, humidity, temperature fluctuations, or other factors, are directly proportional to changes in the model's parameters [1]. With this understanding in mind, examining the vibration as a component of the dynamic

behavior of microdevices is essential for gaining deeper insights into their operation and for optimizing their performance.

In the context of full-field in-plane vibration analysis, the prevailing experimental measurement methods are Laser Doppler Vibrometry (LDV) [2,3] and Electronic speckle pattern interferometry (ESPI) [4,5]. However, despite their accuracy, these methods come with inherent limitations. LDV technique is not suitable for real-time full-field vibration analysis and mode recognition due to the need for the laser beam to scan the surface of the oscillator [3]. Also, in the case of micron-sized devices, LDV is primarily applicable for measuring out-of-plane vibrations [6,7], and its utilization for in-plane investigations becomes a complex process requiring additional optical configurations [8,9]. ESPI and other interferometry techniques [10,11] are not recommended for in-situ measurements due to their highly sensitive optical setup [12,13]. ESPI also suffers from high speckle noises. Besides these drawbacks, LDV relies on backscattered light, and speckle patterns are based on the surface roughness of the studied sample. MEMS typically have very low roughness, often smaller than the wavelength of light, making them unsuitable for these two methods. Digital Image correlation

* Corresponding author.

E-mail address: mona@optim.mech.eng.osaka-u.ac.jp (M. Yadi).

(DIC) [14,15] technique has also found extensive use in full-field in-plane vibration and dynamic investigations. However, this technique requires calibration, has lengthy computation times, and has reduced precision near boundaries. Mentioned drawbacks prompting the need for the introduction of new approaches to address these challenges. In this paper, the in-plane vibration of a special kind of MEMS named Quartz Tuning Fork is investigated.

Quartz Tuning Forks (QTFs) are commercially available crystal oscillators originally designed for precision timekeeping due to their highly accurate in-plane oscillation frequency. Since their introduction to scanning probe microscopy (SPM) in 1989 [16], they have gained prominence in this field. Recently, the QTF-based atomic force microscopy (AFM) devices offer several advantages over conventional microfabricated cantilevers, boasting high stiffness, a high-quality factor, and self-sensing due to the piezoelectric properties of quartz which eliminates the need for optical detection systems [17]. To adapt QTFs for use as sensors in SPM and more recently in AFM devices, tips are attached to one of their prongs. This tip scans sample surfaces, measuring topography through amplitude or frequency modulation concepts [18]. QTFs enable high-resolution imaging, reaching atomic-level precision, and can detect extremely minute interaction forces, even down to femtonewton-range forces in vacuum environments. They maintain impressive resolution, extending to the range of hundreds of piconewtons in air and liquid environments. The accurate measurement of the force depends on the accurate analysis of the parameters like resonance frequency (f_0) and the quality factor (Q) of the sensor in its operating resonance frequency [19]. However, calculating these parameters poses challenges and has led to discrepancies in the literature.

Because of the constraints of the mentioned experimental methods for analyzing this particular specimen, certain researchers have investigated the utilization of quartz's piezoelectric properties to study QTF dynamics. This involves leveraging the electric current generated on the fork's surface post-vibration. However, the precision of this method is dependent on achieving zero energy loss in the electrical circuit configuration which cannot always be completely compensated [20]. Additionally, this method cannot produce frequency mode shapes, which are crucial for system health checks, choosing the accurate position for attaching the tip to detect lateral or vertical forces [21], and directly analyzing the spring constant of the sensor. Researchers also employed analytical and numerical methods for vibration analysis of QTF. An analytical approach often involves the Euler–Bernoulli beam equation for oscillating beams, where each prong of the QTF is assumed as a free-ended beam, and its vibration behavior is calculated accordingly [22]. Although this approach reduces the burden of experimental analysis, it may lack accuracy as it relies on assumptions and encounters complexities due to numerous variables required for analysis, including the geometry of the specimen, density, Young's modulus of all components, temperature, humidity, and probe-sample interactions [20,23]. In the case of numerical methods [24,25], they offer robust capabilities in QTF's dynamics analysis, yet their precision hinges on the designer's accuracy in incorporating the mentioned variables into the simulation. These aspects emphasize the significance of introducing a novel experimental method, which serves to address not only the limitations of the aforementioned experimental approach but also use it as a tool to refine the accuracy of both theoretical and numerical models.

In this study, we proposed a novel method that combines the sampling moiré (SM) technique with stroboscopic technology to explore the full-field in-plane vibration of QTF when subjected to force or vibration. Given the QTF's minute size and high-speed vibration, we have devised a specialized optical setup, integrating a microscope with a stroboscopic illumination system, to capture images of the QTF in motion. These recorded images are then meticulously processed to discern vibration patterns, providing comprehensive insights into the QTF's dynamic behavior, including surface displacement and frequencies. The whole system is named Stroboscopic Sampling Moiré Microscope (SSMM)

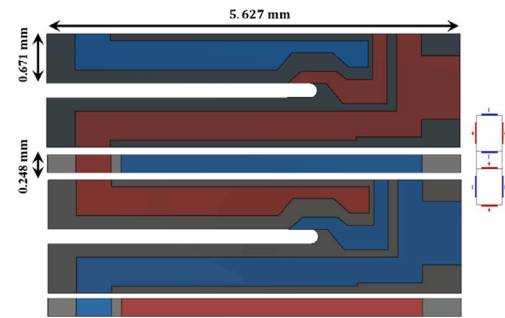


Fig. 1. QTF with coated electrodes.

which covers the whole concept behind this technique. Notably, our approach offers a precise understanding of QTF dynamics utilizing a straightforward optical arrangement. The superior accuracy of SM, compared to other non-contact methods, significantly enhances vibration detection. Furthermore, the proposed method eliminates the need to employ specimen-specific parameters like geometry or material properties such as density, elasticity, and damping ratio for dynamic property analysis, resulting in swift analysis times. Moreover, this methodology is adaptable to various kind of MEMS mechanical transducers compatible with the sample preparation protocol, broadening its applicability.

The outline of this paper is as follows: In the methods Section 2, we discuss the steps towards the full-field in-plane displacement measurement through the theory of the SM method 2.1 and stroboscopic technique 2.2. Experiment setup 2.3 and sample preparation method 2.4 are also discussed in this section. The results are discussed in detail in Section 3. Whole study and future works are discussed and concluded in Section 4.

2. Methods

2.1. Sampling moiré

Fig. 1 depicts a 3D model of the (AB38T-32.768 kHz) QTF, which is used in this study. The QTF is equipped with gold electrode coatings (blue for negative polarity and red for positive polarity) on all four sides, facilitating its mechanical movement through the application of an electrical field. When voltage is applied to the electrodes, the QTF vibrates with the highest amplitude corresponding to its first in-plane resonance frequency.

Fig. 2 illustrates the SM steps for acquiring the in-plane deformation of the QTF during its vibration. This technique involves etching square patterns with a specific pitch size (P) onto the surface of the sample as depicted in Fig. 2(a). The images captured from the sample surface are stored in a buffer and subsequently transferred to a computer for post-processing. To calculate displacements in the y and x directions, smoothing is performed in the respective x or y direction as shown in Fig. 2(b). Down-sampling is then applied to all pixel values of only one recorded image, resulting in new brightness data for that specific frame. These data are utilized for phase extraction and displacement analysis of the sample as demonstrated in Fig. 2(c) and further explained in detail by the authors in [26,27]. The determination of the full-field displacement (h) of the QTF during its vibration is accomplished using Eq. (1), where $\Delta\phi$ corresponds to the phase difference between the recorded images before and after deformation.

$$h = P \left(\frac{\Delta\phi_m}{2\pi} \right) \quad (1)$$

To measure the vibration frequency of an oscillator, based on Nyquist–Shannon theorem, the sampling rate of the oscillation signal should be at least twice the expected frequency. In the case of the QTF

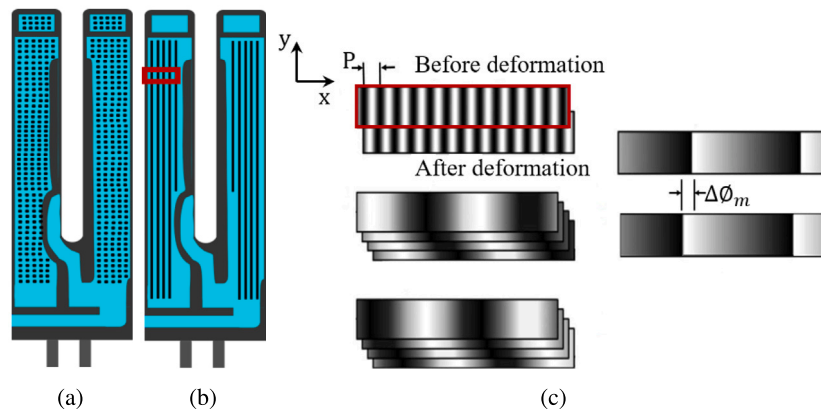


Fig. 2. SM method on QTF's deformation analysis: (a) Captured image of QTF; (b) Smoothing procedure in the y direction; (c) Phase reconstruction.

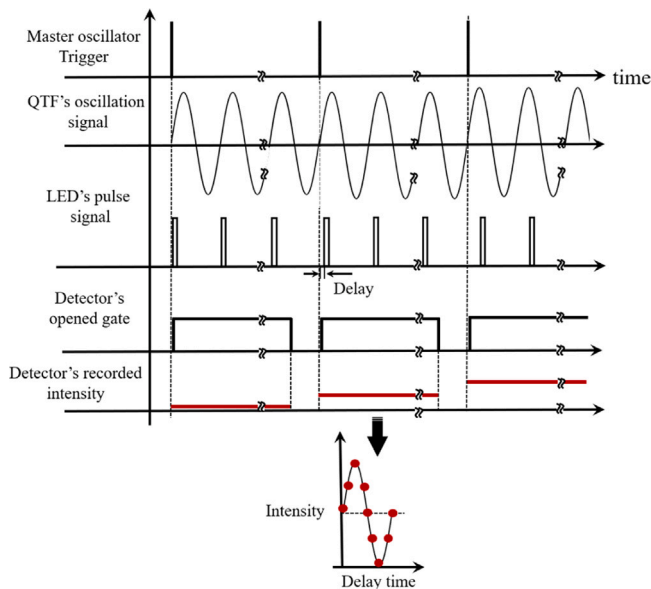


Fig. 3. Concept of stroboscopic technique.

we used in our experiment, the first resonance frequency is located at 32.768 kHz so, for extracting the frequency mode shape and vibration amplitude using SM method, the sampling amount must be more than 66 kHz. This means a high-speed camera with more than 66k frames per second (fps) would be needed to take samples of QTF's vibration. Currently, the best high-speed cameras can cover up to 100k fps which is not good enough for sampling higher frequencies of the QTF and other kinds of MEMS. For this very reason, a stroboscopic method is used for freezing the QTF in a specific position of its vibration using ultra-sharp LED pulse light.

2.2. Stroboscopic technique

Fig. 3 illustrates the concept of the stroboscopic technique. The figure shows the QTF's oscillation signal, displaying a sinusoidal pattern, and the periodic pulse signal of the LED used to illuminate the vibrating QTF. It also depicts the detector's gate's operation, resembling a CCD camera's exposure time. Additionally, the trigger signals of the master oscillator, which synchronize the aforementioned signals, are shown.

The stroboscopic technique, as depicted in this schematic, involves using periodic strobe light flashes synchronized with an object's oscillation frequency. This synchronization creates the illusion that the object is stationary. In Fig. 3, after the master oscillator generates the first

trigger, the sine signal is applied to the QTF, causing it to oscillate. Simultaneously, the pulsed LED light illuminates the QTF during its oscillation. This synchronization effectively freezes the motion of the QTF at a specific position. Extending the camera's exposure time allows for the capture of multiple averaged, frozen images of the QTF in that exact position. During this averaging process, brightness increases, enhancing the signal-to-noise ratio (SNR) of the recorded images. This is particularly beneficial when light intensity is insufficient due to the sharpness of the strobe pulse, which is necessary for recording the high-frequency vibrations of the oscillator. Critical to this configuration is the synchronization of these three signals. Successful synchronization enables the shifting of the strobe pulse's phase which will be added to the system with a new trigger signal generated by the master oscillator. This phase shift allows for capturing images depicting the QTF's vibration throughout an entire oscillation cycle. In fact, by altering the phase of the strobe signal (introducing a time delay) and shifting it through different points of the oscillation time, as demonstrated in Fig. 3, multiple distinct images of the QTF are recorded. Each image corresponds to a different position within one cycle of the QTF's oscillation. This phase shifting of the pulse signal continues until the recorded intensity data covers the entire cycle of the QTF's oscillation.

2.3. Experiment setup

The entire schematic of the SSMM experimental setup is presented comprehensively in Fig. 4, where the upper section pertains to the optical setup, while the lower portion shows the logical and electrical configuration of the system. To manage the operation, two function generators (FG1: Agilent 33210 A, FG2: Kikusui FGA5050) are deployed. FG1 is responsible for generating input sinusoidal signals for the QTF. The signal amplitude is selected to induce maximum vibration amplitude in the QTF, facilitating the evaluation of the proposed technique's feasibility. Simultaneously, FG2 generates pulse signals to drive the strobe. To ensure precise synchronization between these generators, a master oscillator was separately applied to FG1 as a 10 MHz clock named option 001. This clock guarantees a phase resolution of 0.001 degrees and an accuracy of 20 ns. Synchronization between two FGs was achieved through a custom LabVIEW program, granting precise control and coordination over signal specifications as well as timing and phase relationships between the two signal sources. In this method, the burst function was configured to generate an infinite number of cycles, facilitating dynamic adjustments and control of the two signals. A user-friendly interface allowed users to set triggers according to their preferences, enabling seamless customization and synchronization of the signals generated by both function generators.

The output signal from the QTF driver is then directed to the QTF through its electrodes, causing vibration of the specimen. On the other hand, the external signal from the strobe driver is employed to activate

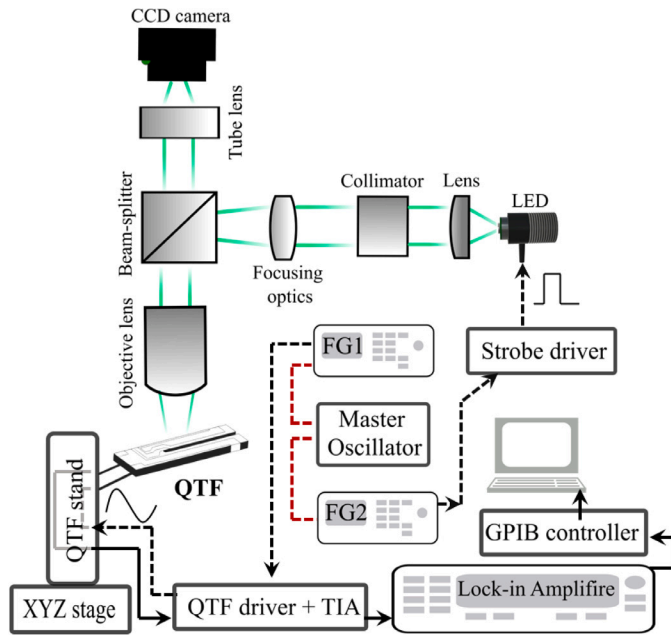


Fig. 4. Schematic of experimental setup.

the LED, generating the necessary light pulses. Imaging is executed through the optical setup, capturing the relevant data. Subsequently, the electric charge generated on the surface of the QTF is routed back to the QTF driver. This charge is then converted into voltage using a transimpedance amplifier (TIA), rendering it readable for the lock-in amplifier (Stanford research SR844 RF). The utilization of a lock-in amplifier serves the essential purpose of precisely extracting and quantifying both the amplitude and phase of the voltage generated by QTF. This voltage signal, typically obscured by background noise and interference, is effectively isolated and analyzed with the assistance of a reference signal originating from FG1. The acquired data is then saved to a computer through using a GPIB controller/interface (National Instruments GPIB-USB-HS). The optical and electrical configurations will be explained in detail in Sections 2.3.1 and 2.3.2.

2.3.1. Optical setup

In stroboscopic applications, the choice of illumination source plays a pivotal role, and certain characteristics are deemed ideal for optimal performance. These attributes include high optical intensity, narrow spectral width, a central wavelength within the objective's range, and a coherence length smaller than the objective's thickness. While lasers often meet these criteria, they can introduce unwanted interferences [11]. For this study, a 505 nm wavelength Light Emitting Diode (LED) (Thorlabs M505L4) with a maximum continuous wave (CW) current of 1000 mA was selected as the illumination source. This LED satisfies the aforementioned requirements, making it a cost-effective and suitable alternative [11].

As it is shown in Fig. 5 an aspheric condenser lens (Thorlabs ACL1815U-A) was chosen to collimate the light. This collimated light was then coupled into an optical fiber (Thorlabs FT600UMT) using a collimator (Thorlabs F810SMA-543). This configuration offers flexibility in the setup and facilitates the use of a photodetector for checking the pulse profile. To further control the amount of light reaching the sample and enhance image contrast and resolution, the collimated light passed through an aperture and lens combination. The beam of light was then directed using a cubic beam splitter (Thorlabs CCM1-BS013) towards an objective lens (Nikon MRL00042) positioned in proximity to QTF. Subsequently, the reflected light from the surface of the QTF was directed to a CCD camera (The Imaging Source DMK33ux178 with

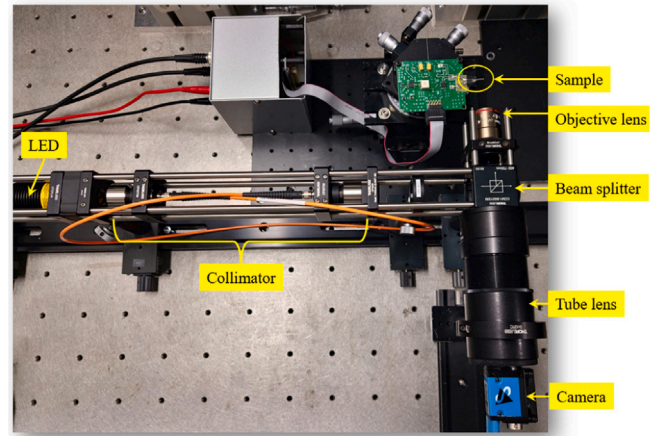


Fig. 5. Optical setup.

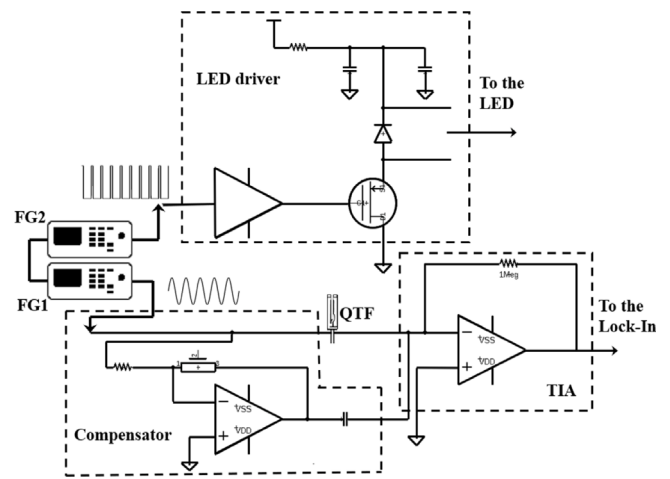


Fig. 6. Electric setup.

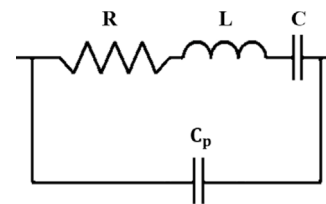


Fig. 7. QTF's equivalent circuit.

a resolution of $3,072 \times 2,048$ pixels). This path was achieved by passing the light through a tube lens (TTL200-A), due to the infinity focal length of the objective lens. In microscopy, the camera's performance is dictated by the Nyquist–Shannon theorem. This theorem specifies that to accurately resolve spatial features with a frequency f the spatial sampling rate must exceed $2f$. In the context of microscopy, the Nyquist frequency (or Nyquist limit) is defined as half the camera's sampling rate, which is essentially determined by the pixel size. In practical terms, this means that to capture the smallest details effectively, a minimum of two pixels is needed for each detail or each line pair of optical resolution. Therefore, for a microscope camera, the Nyquist–Shannon theorem requires:

$$M_{obj} \times M_{cam\ lens} \times d_0 \geq 2P_{sensor} \quad (2)$$

$$d_0 = 1.22 \times \frac{\lambda}{NA} \quad (3)$$

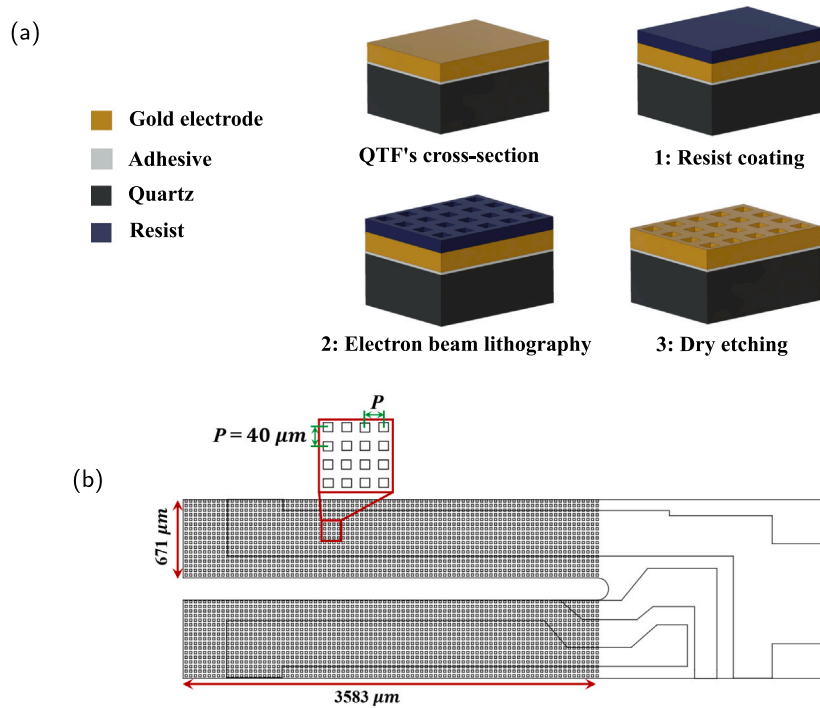


Fig. 8. Sample preparation: (a) Etching steps from 1 to 3; (b) Etched area of the QTF's surface with 40 μm pitch size.

In Eq. (2), d_0 represents the resolution of the objective lens, and it can be computed using Abbe's equation (Eq. (3)). Here, M_{obj} and $M_{cam\ lens}$ denote the magnifications of the objective and camera lens, respectively. Additionally, P_{sensor} signifies the pixel size of the camera sensor, λ is the wavelength of the light source, and NA stands for the numerical aperture of the objective lens. In the proposed setup to ensure that the objective's resolution requirements are met, the camera sensor pixel size (P_{sensor}) should ideally be equal to or smaller than approximately 12 μm which comfortably satisfies due to the 2.4 μm camera's pixel size. This information is particularly crucial during sample preparation in which the pattern size should be chosen accurately (See Section 2.4).

2.3.2. Electrical configuration

The upper part of Fig. 6 illustrates a simple, self-constructed LED driver intended for generating sharp pulses [28]. It employs a gate driver, which is pivotal for delivering the necessary current to switch a power MOSFET on and off swiftly. The gate driver must have a rise and fall time that is quicker than the MOSFET's switching speed to avoid any lag in response. Additionally, the circuit incorporates a capacitor discharge mechanism. This mechanism charges the capacitor to a high voltage and then rapidly discharges it through the LED, resulting in a high-current pulse. This setup requires a robust high voltage DC source and a powerful current switch, such as the MOSFET, to manage the capacitor's discharge effectively. Lastly, a parallel fast diode is included to safeguard the LED against any potential reverse voltage damage. This ensures that the LED only receives the correct forward voltage and is protected from any fluctuations that might occur in the circuit. Moreover, the diode included in the design is chosen for its quick recovery time, which is vital to prevent the shoot-through phenomenon—a condition where both the MOSFET and the diode are conducting simultaneously, which could lead to circuit damage.

The lower portion of Fig. 6 is dedicated to the QTF driver. In the absence of the compensator, the signal from the FG1 would be directly transmitted to one electrode of the QTF, causing it to vibrate. The quartz-induced current would then flow from the other electrode of the

QTF to the TIA. The TIA converts this current to a voltage signal with the help of a 1 M Ω feedback resistor.

However, this straightforward measurement of oscillation amplitude via the QTF current is complicated by parasitic capacitance, which can inaccurately reflect the true amplitude. When FG1's signal frequency sweeps around the resonance frequency of the QTF, the parasitic capacitance can introduce asymmetry and shifts in the frequency response [29]. Fig. 7 presents the equivalent electrical circuit of the QTF, following a Butterworth-Van Dyke model. This model includes a series configuration of resistance, inductor, and capacitor to represent the QTF's oscillatory electrical behavior, along with a parallel capacitance accounting for parasitic effects from contacts, cables, etc.

To mitigate the distortive effects of parasitic capacitance, the circuit includes a compensator. This compensator is designed to generate a current equal in magnitude but opposite in phase (180 degrees shifted) to the current produced by the parasitic capacitance (C_p). When these two currents are superimposed, they effectively cancel each other out, thereby reducing the impact of parasitic capacitance on the signal and enhancing the accuracy of the frequency response measurement. Although achieving one hundred percent compensation for parasitic capacitance is never entirely possible, employing the compensator yields better results than not using one at all.

2.4. Sample preparation

Fig. 8(a) illustrates the cross-sectional view of a small part of the QTF utilized in this study, where gold electrodes are affixed to the surface of the quartz using an adhesive. The precise thickness of the gold and adhesive layers is not provided by the manufacturer, necessitating a degree of trial and error to develop an effective recipe for etching patterns on the QTF's surface. This process is critical for employing the SM method, which requires a uniform square pattern across the entire surface of the sample.

As shown in the figure, the sample preparation process for the SM method is defined in several steps, labeled from "1" to "3". Initially, the photoresist material ZEP520 A (ZEP: Styrene Methyl Acrylate-based positive e-beam resist), with a depth of 300 nm, is coated on the

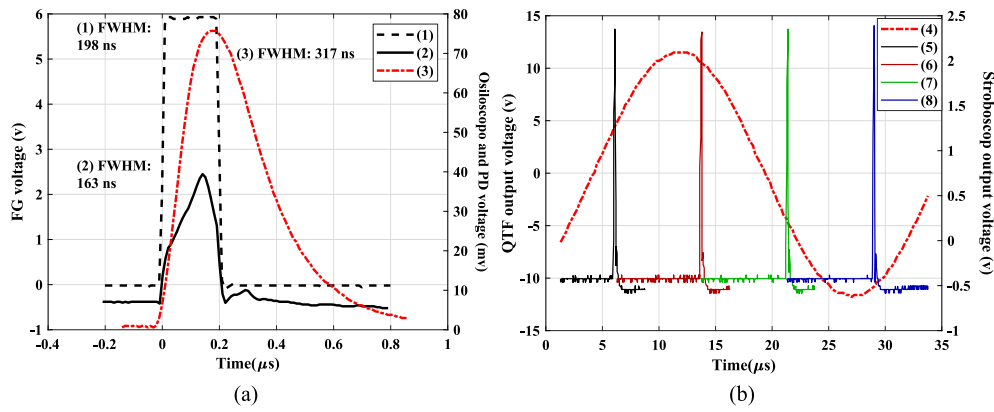


Fig. 9. Stroboscopic driver generated pulse: (a) Pulse width; 1: FG2 output 2: Photodetector output 3: Oscilloscope output (b) Synchronization test; 4: QTF voltage 5: Strobe pulse with phase zero 6: $\pi/2$ 7: π and 8: $3\pi/2$.

QTF’s surface, as depicted in step “1” (Opticoat spin coater (MS-A150) is used). This base layer is essential for subsequent pattern creation. Next, using an electron beam lithography device like the Elionix ELS-100T, square patterns with $20\ \mu\text{m}$ sides and a pitch of $40\ \mu\text{m}$ are crafted, as visualized in step “2”. This process took one and a half hours. The reactive ion etching process follows, utilizing a device such as the Samco-UCP RIE-10NR to etch the square patterns into the QTF’s gold electrodes. This etching takes 45 min at a rate of 8.43 nm/min, represented in step “3”. In order to clean the samples from the remaining resist material the whole sample was deepened into a 3:2 mixture of dimethyl sulfoxide and N-methyl-2-pyrrolidone for 12 h and then cleaned with a UV ozone cleaning device (Samco UV-1). To save time and money, this process can be done by the manufacturer during affixing electrodes on the surface of the specimen. Fig. 8(b) showed the etched area on the surface of QTF.

3. Results and discussion

In Fig. 9(a) the first waveform, indicated as “1”, displays a Full Width at Half Maximum (FWHM) value of 198 ns, which corresponds to the pulse generated by FG2, as shown in the first part of the graph. The second waveform, marked as “2”, illustrates the FWHM of the LED output pulse captured by a photodetector (DET25K/M with a rise time of 50 ns) presented in the second segment of the graph. Additionally, the third part of the graph, labeled as “3”, represents the output signal of the strobe driver, evaluated using an oscilloscope.

Analyzing the data acquired from the photodetector, it is anticipated that the pulse directed to the sample will have a width with a FWHM of 163 ns.

Fig. 9(b) displays the results of an experiment designed to verify the adequacy of the pulse width to encompass the entire cycle of a QTF’s vibration at its first resonance frequency. Additionally, it aims to assess the synchronization between two FGs. To achieve this, the phase of the pulse signal was altered in increments of 90 degrees. Fig. 9(b) captures one complete cycle of the QTF’s drive signal, as shown in trace “4”. Simultaneously, the pulse emanating from the strobe driver, previously shown in trace “2” of Fig. 9(a), is depicted in trace “5” as being programmatically shifted by 90 degrees at each stage (shown in trace 6, 7 and 8) until it spans the full cycle. The figure clearly indicates that the pulse width produced by the in-house built strobe driver is sufficient for the sampling rate to fully capture the QTF’s vibration cycle at its initial resonance frequency of 32.768 kHz. This ensures that the experimental setup can effectively monitor the QTF’s vibration within the specified parameters. New research has recently demonstrated that LEDs have the potential to provide 7 ns pulse widths, enabling the measurement of oscillations in the hundreds of MHz range for certain MEMS mechanical transducers [30]. For transducers operating at even

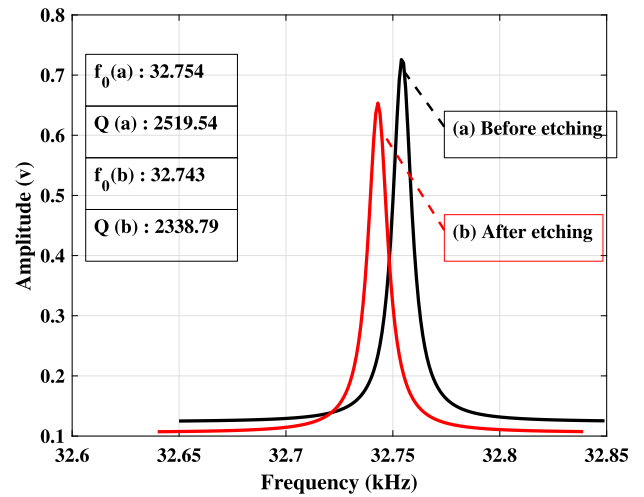


Fig. 10. Resonance frequency and quality factor of the QTF before (a) and after (b) etching.

higher frequencies, laser pulses, which offer narrower pulse widths, can be employed for more accurate measurements.

Fig. 10 referred to shows the results of the electrical approach used to assess the mechanical properties of QTF (f_0 and Q). This method involves an analysis of the QTF’s electrical response, which is determined by the electric current it generates and its modal characteristics. Before integrating the QTF into the SSMM setup, tests are performed to evaluate f_0 and Q values before and after etching, observing the effects of the etching process on the QTF’s dynamic behavior. The electrical response is assessed by varying the drive frequency of the QTF from 32.6 kHz to 32.8 kHz, and the resulting data from the lock-in amplifier is illustrated in Fig. 10. The data allows for the straightforward calculation of the resonant frequency and quality factor; the peak indicates f_0 , and the Q , an indicator of the resonator’s bandwidth relative to its central frequency, is computed using the Eq. (4), where Δf is the resonance width at FWHM.

$$Q = \frac{f_0}{\Delta f} \quad (4)$$

The (a) plot, reveals a slight discrepancy in f_0 value when compared with the manufacturer’s data, attributed to the QTF’s operation in air rather than a vacuum and the incomplete energy compensation by the compensator, leading to minor measurement errors. Nonetheless, the new f_0 and Q (related to (b) plot) values show negligible alterations in the QTF’s dynamics, indicating that the etching process had minimal

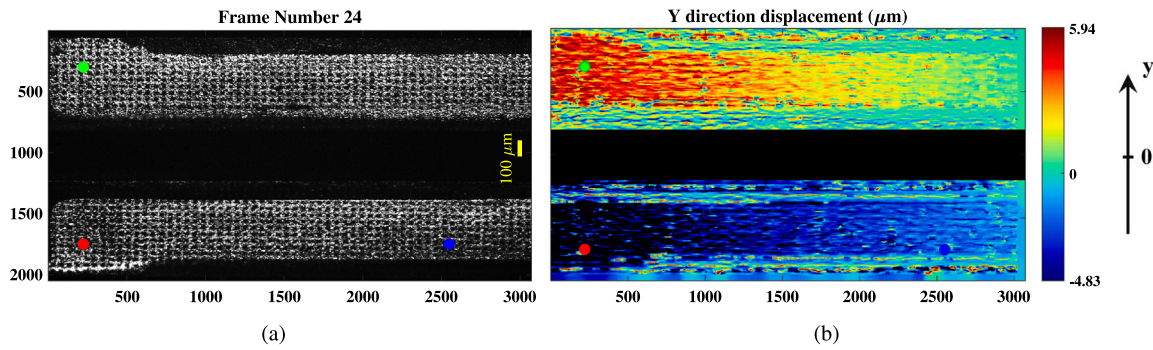


Fig. 11. Y-Directional displacement measurement of QTF using SSMM: (a) QTF image captured at 0.42 s during a one-second recording time; (b) Displacement distribution at the first resonance frequency.

impact on the sample's mass and the symmetry of the QTF prongs. These findings will be compared with results obtained using the SSMM technique.

There are two methods employed in SSMM to capture in-plane vibration behavior of the QTF during its oscillation. The first method involves adjusting the phase of the strobe signal in intervals to cover an entire cycle of the vibration as explained in detail in Section 2.2. This allows for the CCD exposure to be open for a sufficient duration, resulting in images with high SNR. The second method introduces a frequency difference between the strobe signal and the QTF driving signal, creating a beat frequency effect. For example, a 3 Hz frequency difference causes the QTF's vibration to appear as if it is vibrating at 3 Hz. In this study, we utilized the second approach to investigate the in-plane vibration of the QTF due to its simplicity.

The experimental conditions in the SSMM setup, controlled by a customized LabVIEW program, were configured as it is shown in Table 1.

In this experiment, after confirming the f_0 of the QTF, as shown in Fig. 10, we aligned the QTF's driving frequency to 32.743 kHz. The strobe pulse frequency was set to be 3 Hz lower than the QTF driver's frequency. With this configuration, we aimed to detect a beat frequency of 3 Hz using the proposed method. Fig. 11(a) illustrates the recorded brightness data of the QTF, corresponding to the 24th camera frame and the three dots, marked in red, blue, and green, represent the locations on the sample under investigation. In Fig. 11(b), we observe the displacement distribution of the QTF corresponding to the same frame or time period within one cycle of the QTF's vibration which also depicts the first resonance frequency mode shape. This result depicts almost the same behavior that is expected to be seen in a free-end beam. To gain a clearer understanding of these results, Fig. 12 presents three waveforms that depict the vibration amplitudes of the QTF at the positions corresponding to the three dots. Three dots located in this figure show the corresponding result calculated in the time domain related to frame number 24. As anticipated, we detect three cycles of vibration within one second, aligning with the applied beat frequency. These three vibration cycles account for 91.62 microseconds of the QTF's oscillation time domain.

A comparison between the red and blue dots reveals variations in the amplitude of vibration at two distinct locations along the length of the QTF's prong. Meanwhile, a comparison between the red and green dots highlights the phase difference between the vibrating signals of the two prongs. Fig. 11(b) demonstrates that such investigations can be seamlessly conducted across the entire surface of the QTF simultaneously, facilitating the detection of mode shapes and simultaneous full-field displacement measurement.

Fig. 13(a) provides a more detailed view of the data presented in Fig. 10 plot (b). In Fig. 13(a), the red plot represents the QTF's generated current (converted to voltage using TIA shown in Fig. 6) obtained using lock-in amplifier during the sweep frequency of the QTF's driving signal. According to the electrical behavior of the QTF,

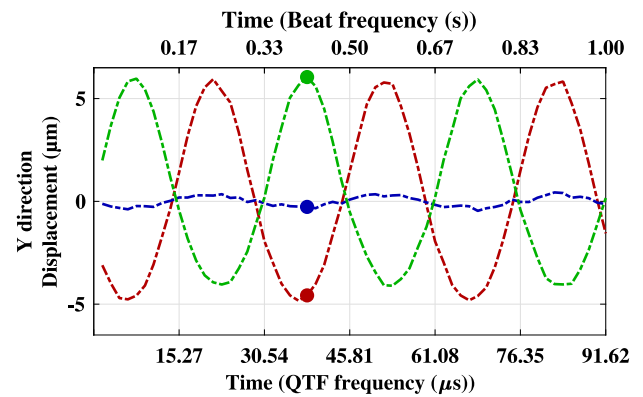


Fig. 12. Comparison of vibration amplitude of three dots located in Fig. 11(a).

as explained earlier, a pure Lorentzian plot should be observed, but the symmetry of the plot is disrupted due to electrical losses. The compensator circuit was applied to partially compensate the energy loss and the recorded results are fitted to a Lorentzian function, as indicated by the black plot. To compare these results with the SSMM data, we conducted a similar frequency sweep within the same range as in the previous experiment. This time, we measured the displacement at a location near the end of the prong, chosen for its significant displacement, and recorded the change in displacement at each frequency. Fig. 13(b) displays the recorded results. In this figure, the red data, representing the actual displacement values calculated using the SSMM system, exhibits a pure Lorentzian shape, perfectly matching the black plot which shows the fitted results to a Lorentzian function. These results underscore the effectiveness of the SSMM method in analyzing the dynamic parameters of the QTF. As depicted in Fig. 13, while the f_0 values are nearly identical in both methods, the Q differs significantly and is inaccurately determined using the electrical approach due to the mentioned drawbacks of electrical analysis.

It is noteworthy that SSMM can also be directly used to measure the resonance frequency of specimens with unknown resonant frequencies, following the same approach illustrated in 13(b). To enhance analysis speed in this case, a small section of the recorded images – containing at least 3 to 4 square patterns in both the x and y directions – can be sufficient for applying the SM method and measuring the oscillator's resonance frequencies.

A repeatability test was conducted to measure the standard deviation (SD) of f_0 , Q , and the measured amplitude (A) using the proposed SSMM method. The results are summarized in Table 2. In this particular test, an error of 0.364 μm was measured, which is less than 1/100th of the pitch size of the square patterns. To reduce the error and improve measurement resolution, a smaller pitch size is required, as mentioned

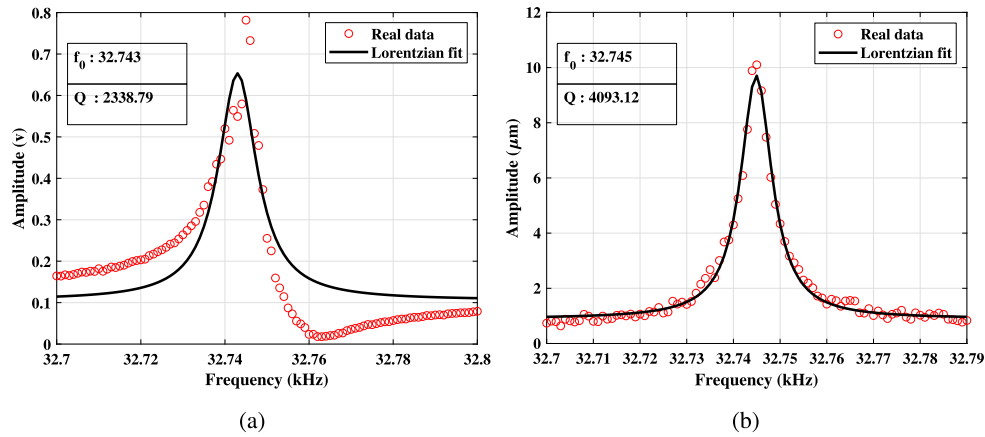


Fig. 13. Dynamic measurement using: (a) QTF's generated current; (b) SSMM analysis.

Table 1

Experiment condition.

QTF driving frequency	32.743 kHz
Strobe pulse frequency	32.740 kHz
Beat frequency	3 Hz
Recording time	1 s
Frame speed	60 frames per second

Table 2

Repeatability test conditions and results.

Number of tests	10
Temperature	23.2 °C
Humidity	39%
SD (f_0)	0.1414 Hz
SD (Q)	211.4
SD (A)	0.364 μm

in Eq. (1). For example, a pitch size of 40 nm can reduce displacement detection error to under 0.4 nm, enabling the measurement of higher frequencies at lower amplitudes. This pitch size is achievable with the Elionix ELS-100T electron beam lithography device used in the experiment, which can produce a minimum line width of 5 nm. In a QTF-based AFM setup, where the QTF sensor oscillates at the sub-nanometer level, this factor should be considered when selecting the pitch size during sample preparation.

4. Conclusion

In this study, we introduced a novel technique that combines the sampling moiré (SM) method with stroboscopic technology to investigate the in-plane vibration of a specific kind of MEMS mechanical transducer named Quartz Tuning Fork (QTF). By leveraging a specialized optical setup comprising a microscope and stroboscopic illumination system, we captured high-speed images of QTF motion. Through meticulous image processing, we obtained comprehensive insights into QTF dynamic behavior, including surface displacement and frequencies. This method, named Stroboscopic Sampling Moiré Microscope (SSMM), offers a precise understanding of QTF dynamics without the need for considering specimen-specific parameters such as geometry or material properties, thereby streamlining analysis processes. The proposed technique not only addresses the limitations of existing experimental methods but also serves as a valuable tool for refining theoretical and numerical models of MEMS transducer dynamics. Its adaptability to various MEMS sensors further enhances its utility, promising broader applicability across the field. In addition to the aforementioned advantages, achieving precise deformation analysis at sub-nanometer scales using these techniques necessitates smaller pitch sizes of square patterns added to the sample's surface. However, this may pose a

challenge, as spatial features within the field of view of the CCD camera may not be accurately resolved if the appropriate optics are not used for capturing images. Furthermore, the color of the samples presents another obstacle, as brighter colors can enhance the Signal-to-Noise Ratio in recorded images, thereby increasing the accuracy of deformation analysis. Consequently, it is preferable for samples to have a brighter color, especially when sub-nanometer deformation accuracy is crucial. In future work, this technique will be used to measure spring constants, providing another essential dynamic parameter. Besides, the methods will be applied to evaluate the quality of MEMS mechanical transducers based on the measured dynamic properties. Applying SSMM to a tip-attached QTF within a real AFM setup by using etched square patterns with a smaller pitch size would be an interesting direction for further study. This approach could reveal how the addition of the tip alters the sensor's frequency mode shapes and dynamic parameters, and how these changes impact the imaging system's resolution.

CRediT authorship contribution statement

Mona Yadi: Writing – original draft, Validation, Software, Methodology, Investigation, Formal analysis, Data curation. **Tsutomu Ueno-hara:** Writing – review & editing, Supervision. **Yasuhiro Mizutani:** Supervision, Resources, Funding acquisition. **Yoshiharu Morimoto:** Supervision. **Yasuhiro Takaya:** Supervision, Resources, Funding acquisition.

Declaration of competing interest

The authors declare that they have no known competing financial interests or personal relationships that could have appeared to influence the work reported in this paper.

Acknowledgments

This research with proposal number JPMXP1223OS1043 was supported by the Center of Advanced Research Infrastructure for Materials and Nanotechnology (ARIM).

References

- [1] Jassim Z, Ali N, Mustapha F, Jalil NA. A review on the vibration analysis for a damage occurrence of a cantilever beam. *Eng Fail Anal* 2013;31:442–61.
- [2] Zhong Y, Zhang G, Leng C, Zhang T. A differential laser Doppler system for one-dimensional in-plane motion measurement of MEMS. *Measurement* 2007;40(6):623–7.
- [3] Arabi M, Gopanchuk M, Abdel-Rahman E, Yavuz M. Measurement of in-plane motions in MEMS. *Sensors* 2020;20(12):3594.
- [4] Aswendt P, Schmidt C-D, Zielke D, Schubert S. ESPi solution for non-contacting MEMS-on-wafer testing. *Opt Lasers Eng* 2003;40(5–6):501–15.

- [5] Engelsberger J, Nösekabel E, Steinbichler M. Application of interferometry and electronic speckle pattern interferometry (ESPI) for measurements on MEMS. In: *Fringe 2005: the 5th international workshop on automatic processing of fringe patterns*. Springer; 2006, p. 488–93.
- [6] Osten W, Duparre A, Furlong C, De Wolf I, Asundi A, Korner K, et al. *Optical inspection of microsystems*. CRC Press; 2018.
- [7] Rembe C, Kant R, Muller RS. Optical measurement methods to study dynamic behavior in MEMS. In: *Microsystems engineering: metrology and inspection*, vol. 4400, SPIE; 2001, p. 127–37.
- [8] Kim MG, Jo K, Kwon HS, Jang W, Park Y, Lee JH. Fiber-optic laser Doppler vibrometer to dynamically measure MEMS actuator with in-plane motion. *J Microelectromech Syst* 2009;18(6):1365–70.
- [9] Herth E, Lardet-Vieudrin F, Deux F, Valbin L, Algré E, Schell J, Steger H. Detection of out-of-plane and in-plane (XYZ) motions of piezoelectric microcantilever by 3D-Laser Doppler Vibrometry. In: 2016 symposium on design, test, integration and packaging of MEMS/MOEMS. DTIP, IEEE; 2016, p. 1–4.
- [10] Conway JA, Osborn JV, Fowler JD. Stroboscopic imaging interferometer for MEMS performance measurement. *J Microelectromech Syst* 2007;16(3):668–74.
- [11] Ventura LG, Wolschke S, Skupsch C, Berndt D. Development of an illumination module for stroboscopic phase-shift interferometry on MEMS devices. In: *Optical measurement systems for industrial inspection XI*, vol. 11056, SPIE; 2019, p. 1084–97.
- [12] Kurth S. *Interference microscopic techniques for dynamic testing of MEMS*. Germany: Chemnitz University of Technology; 2002.
- [13] Kopec M, Brodecki A, Kukla D, Kowalewski Z. Suitability of DIC and ESPI optical methods for monitoring fatigue damage development in X10CrMoVNb9-1 power engineering steel. *Arch Civ Mechan Eng* 2021;21:1–13.
- [14] Serio B, Hunsinger J, Cretin B. In-plane measurements of microelectromechanical systems vibrations with nanometer resolution using the correlation of synchronous images. *Rev Scient Instrum* 2004;75(10):3335–41.
- [15] Teyssieux D, Euphrasie S, Cretin B. MEMS in-plane motion/vibration measurement system based CCD camera. *Measurement* 2011;44(10):2205–16.
- [16] Günther P, Fischer UC, Dransfeld K. Scanning near-field acoustic microscopy. *Appl Phys B* 1989;48:89–92.
- [17] González L, Oria R, Botaya L, Puig-Vidal M, Otero J. Determination of the static spring constant of electrically-driven quartz tuning forks with two freely oscillating prongs. *Nanotechnology* 2015;26(5):055501.
- [18] Giessibl FJ. The qPlus sensor, a powerful core for the atomic force microscope. *Rev Scient Instrum* 2019;90(1).
- [19] Ooe H, Sakuishi T, Nogami M, Tomitori M, Arai T. Resonance frequency-retuned quartz tuning fork as a force sensor for noncontact atomic force microscopy. *Appl Phys Lett* 2014;105(4).
- [20] Oria R, Otero J, González L, Botaya L, Carmona M, Puig-Vidal M. Finite element analysis of electrically excited quartz tuning fork devices. *Sensors* 2013;13(6):7156–69.
- [21] Ruppert MG, Martin-Jimenez D, Yong YK, Ihle A, Schirmeisen A, Fleming AJ, et al. Experimental analysis of tip vibrations at higher eigenmodes of QPlus sensors for atomic force microscopy. *Nanotechnology* 2022;33(18):185503.
- [22] Patimisco P, Sampaolo A, Mackowiak V, Rossmadl H, Cable A, Tittel FK, et al. Loss mechanisms determining the quality factors in quartz tuning forks vibrating at the fundamental and first overtone modes. *IEEE Trans Ultrason Ferroelectr Freq Control* 2018;65(10):1951–7.
- [23] Kim B, Jahng J, Khan RM, Park S, Potma EO. Eigenmodes of a quartz tuning fork and their application to photoinduced force microscopy. *Phys Rev B* 2017;95(7):075440.
- [24] Dagdeviren OE, Schwarz UD. Optimizing qPlus sensor assemblies for simultaneous scanning tunneling and noncontact atomic force microscopy operation based on finite element method analysis. *Beilstein J Nanotechnol* 2017;8(1):657–66.
- [25] Falter J, Stieffermann M, Langewisch G, Schurig P, Hölscher H, Fuchs H, Schirmeisen A. Calibration of quartz tuning fork spring constants for non-contact atomic force microscopy: direct mechanical measurements and simulations. *Beilstein J Nanotechnol* 2014;5(1):507–16.
- [26] Yadi M, Morimoto Y, Ueki M, Takaya Y. In-plane vibration detection using sampling moiré method. *J. Phys. Photon.* 2021;3(2):024005.
- [27] Ri S, Fujigaki M, Morimoto Y. Sampling moiré method for accurate small deformation distribution measurement. *Exp Mech* 2010;50:501–8.
- [28] Kuniyil Ajith Singh M, Xia W. Portable and affordable light source-based photoacoustic tomography. *Sensors* 2020;20(21):6173.
- [29] González L, Otero J, Cabezas G, Puig-Vidal M. Electronic driver with amplitude and quality factor control to adjust the response of quartz tuning fork sensors in atomic force microscopy applications. *Sensors Actuators A* 2012;184:112–8.
- [30] Real D, Calvo D, Díaz A, Salesa Greus F, Sánchez Losa A. A narrow optical pulse emitter based on LED: NOPELED. *Sensors* 2022;22(19):7683.